Oxygen Evolution

DOI: 10.1002/anie.201304765

In Situ Study of the Gas-Phase Electrolysis of Water on Platinum by NAP-XPS**

Rosa Arrigo, Michael Hävecker, Manfred E. Schuster, Chinmoy Ranjan, Eugen Stotz, Axel Knop-Gericke, and Robert Schlögl*

Water electrolysis is critical for integrating renewable primary electricity into existing energy systems. However, for practical grid-scale application, the performance and stability of the electrolyzers must be improved. Research in materials science tries to improve the efficiency of the process through the development of an electrode with low intrinsic over-potential as well as stability against corrosion induced at the anodic potential of the oxygen evolution reaction (OER)[1–4] during cyclic operation. Knowledge of the structural transformation of the electrocatalyst surface upon OER is essential to design better electrode materials. Pt is one of the most frequently used materials for polyelectrolyte membrane (PEM) fuel cells[5] and has been considered as a model system to study structural transformations upon polarization.[4–11] In aqueous medium, high anodic polarization results in the dissolution of oxygen into the metallic electrode and under extreme conditions, oxygen evolution. That is, the OER occurs only after the appropriate population of oxygen species in Pt has been achieved.[8] Pioneering work by Bockris et al.[6] by means of in situ ellipsometry identified the formation of a PtO_2 phase before OER takes place and subsequent transition to instable PtO_3 as the mechanism of OER.[11] In contrast, ^{18}O experiments aimed to clarify the involvement of the oxide layer for the OER are contradictory.[10,11]

X-ray photoelectron spectroscopy (XPS) was applied early on to study the nature of the anodic oxide at the Pt surface.[7–13] Most of these studies were carried out by coupling electrochemical methods with XPS in an ex situ fashion. For instance, the Pt 4f XP spectra obtained ex situ for the Pt surface after anodic polarization[12,14] show components at the same binding energy (BE) shift as those seen for thermally oxidized Pt under high O_2 pressure or after O_3 treatment[15] and are attributed to a mixture of Pt^{2+} and Pt^{4+}. More recently, an in situ X-ray absorption near-edge spectroscopy (XANES) study of the electrochemical oxidation of Pt nanoparticles in $HClO_4$ has shown that the oxide component in the Pt L_3-XANES spectra, which grew continuously over 30 min, is mainly composed of Pt^{2+}.[16] Interestingly, the onset potential for oxide formation was lower and the growth of the oxide component more rapid on Pt/C than on Pt/Rh, indicating that the energy barrier for oxygen dissolution into the Pt subsurface plays an important role in oxide formation.

Herein we describe our study of the chemical reactivity of the electrode surface under OER for low-temperature gas-phase electrolysis by means of the near-ambient-pressure (NAP)-XPS end-station at the ISISS beamline (HZB/BESSY II).[17,18] Low-pressure gas-phase electrolysis limits the chemical potential of oxygen and offers the possibility that the oxide phase growth is thermodynamically and/or kinetically hindered. In this way the early stages of chemical transformation can be seen and its direct involvement can be evidenced in the electrocatalytic formation of oxygen. Chrono-amperometry (CA) was applied to the electrode system in combination with in situ XPS. The gas composition was continuously monitored by online mass spectrometry (MS). The system under investigation was a Pt/Nafion-based electrode. The Nafion membrane electrolyte is sputter-coated on both sides by the electroactive element (Pt), which functions as a cathode on one side and as an anode on the other.

The morphology and nanostructure of the Pt film were examined before the in situ investigation (Figure 1). The sputter-coated Pt film is not a bulk Pt film but a nanostructured Pt film. Electron micrographs (EM) reported in order of increasing magnification in spatial dimensions provided information about the Pt film from the macroscopic level down to the atomistic level so that the film could be represented in three dimensions. The polycrystalline Pt film is approximately 70 nm thick and is composed of interconnected nanoparticles that form a network with multiple percolation pathways. The typical survey spectrum for the Pt film electrode shows beside peaks due O and Pt core levels also the presence of C and F (Figure S1) verifying the intended porous structure of the Pt required for mass transport.

The cell designed for the in situ investigation is sketched in Figure 2a. The cell has a reservoir for liquid that is leak-

[*] Dr. R. Arrigo, Dr. M. E. Schuster, E. Stotz, Dr. A. Knop-Gericke, Prof. Dr. R. Schlögl
Abteilung Anorganische Chemie
Fritz-Haber-Institut der Max-Planck Gesellschaft
Faradayweg 4–6, 14195 Berlin (Germany)
E-mail: arrigo@fhi-berlin.mpg.de
Dr. M. Hävecker
Helmholtz-Zentrum Berlin für Materialien und Energie, BESSY-II
Albert-Einstein-Strasse 15 12489 Berlin (Germany)
Dr. R. Arrigo, Dr. C. Ranjan, Prof. Dr. R. Schlögl
Max-Planck-Institut für Chemische Energiekonversion
Stiftstrasse 34–36, 45470 Mülheim an der Ruhr (Germany)

[**] We thank Achim Klein-Hoffmann (FHI) for preparation of cross-section TEM samples and Youngmi Yi for help in conventional electrochemical measurements. We thank Dr. Detre Teschner and Dr. Tulio Rocha Costa Rizuti for help in improving the manuscript. We thank Bessy II staff for their continuing support during the XPS measurements. NAP-XPS = near-ambient-pressure X-ray photoelectron spectroscopy.

Supporting information for this article is available on the WWW under http://dx.doi.org/10.1002/anie.201304765.

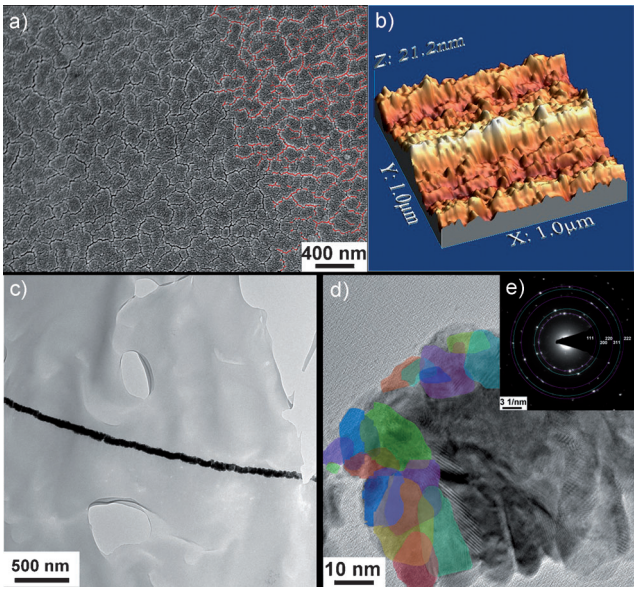

Figure 1. a) SEM image (top view) of the Pt film showing the peculiar morphology of the film with random cracks. The cracks are highlighted in red on the right side to show that the domains are interconnected. b) AFM image provides a three-dimensional representation of the film and evidences the high surface roughness of the 70-nm-thick Pt film (c). d) HRTEM image of the film shows that it is composed of agglomerates of nanoparticles. The colored areas indicate the extension of crystallographic planes belonging to individual particles and shows that the nanoparticles are in contact with each other. This is also indicated by the typical Moiré fringes for overlapping lattice. The film is accommodated on the Nafion surface (top in d) according to its morphology and this gives rise to thickness variation as well as roughness. The very thin region in (d) (10 nm) corresponds to the cracks observed in the SEM image in (a). e) Selected area diffraction (SAD) image shows that the film is polycrystalline metallic Pt.

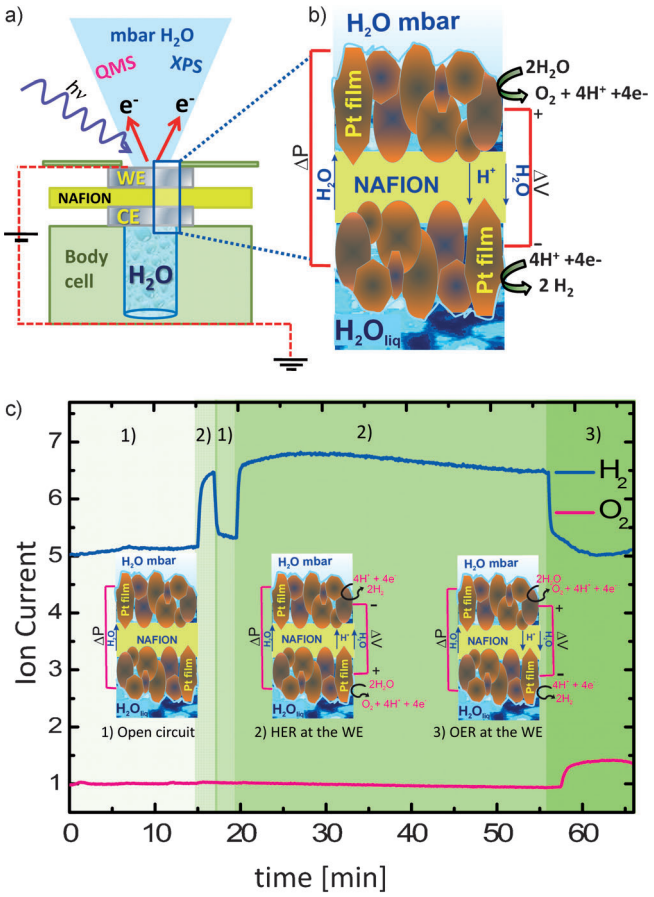

Figure 2. a) The cell for the in situ investigation with a liquid reservoir. b) Due to the pressure difference the water in the liquid reservoir diffuses through the membrane and generates water pressure in the XPS chamber in the range of mbar. The porosity of the Pt film allows the water transport. The electrode exposed to X-rays is the WE. c) Depending on the potential applied at the WE, OER (+2 V), or hydrogen evolution reaction (HER; −2 V) occurs and m/z 2 for H_2 or m/z 32 for O_2 are detected by MS.

proof and sealed with the Pt-coated Nafion membrane which is in direct contact on one side with the liquid water. Liquid water in the reservoir serves two purposes: it supplies the reactant molecules to both the electrodes due to the permeability of the Nafion membrane and the porosity of the Pt film; it also guarantees good hydration of the membrane which is fundamental for achieving good ion conductivity. The electrode directly in contact with the liquid water functions as the counterelectrode (CE), while the electrode exposed to photons is the working electrode (WE). During measurements, the CE Fermi edge (FE) is aligned with the FE of the spectrometer and therefore any potential difference between the two electrodes is observed as a shift in the binding energy (BE) scale of the XPS peak. More information is in Supporting Information (Figure S2).

The sketch in Figure 2b depicts the porous Pt film composed of agglomerated, electrically interconnected nanoparticles. Water transport through the Nafion membrane and the porous film results in a pressure up to 10^{-2} mbar in the XPS chamber. The MS traces of H_2 and O_2 in Figure 2c show the response of the system to the applied potentials. Switching from open-circuit potential (configuration 1 in Figure 2c) to the configuration such that the WE functions as the cathode (configuration 2 in Figure 2c) and back produces an appreciable change in the H_2 trace. When the WE functions as the anode (configuration 3 in Figure 2c), the O_2 trace increases. These results indicate that the in situ cell/electrode assembly works as a functional water-splitting device.

The transformation of the Pt 4f and O 1s spectra during OER at different anodic potential is reported in Figure 3. The corresponding MS signal for O_2 increases when the potential is increased from 2 V to 2.5 V and indicates an increase in the OER rate (Figure 3a): The current is representative of the "mass balance" of the product. The Pt 4f spectra are reported in Figure 3b. Differences in the spectra are described as changes of the three components, Pt1, Pt2, and Pt3. Pt1 corresponds to metallic Pt (71 eV)[9,15] and Pt2 and Pt3 are shifted 0.6 eV and 1.3 eV to higher BE, respectively. The Pt2 component is found on the Pt foil under oxygen at 250 °C and partly persists after exposure to H_2O (Figure S3). This component is attributed to O on Pt as 2D surface oxide clusters.[9] The Pt3 component at 72.5 eV is observed also on electrochemically oxidized Pt foil in acidic media together with a component Pt4 at 74.5 eV (Figure S5C).[6,9,15] These two components are attributed to Pt species with a formal valence of +2 and +4, respectively.

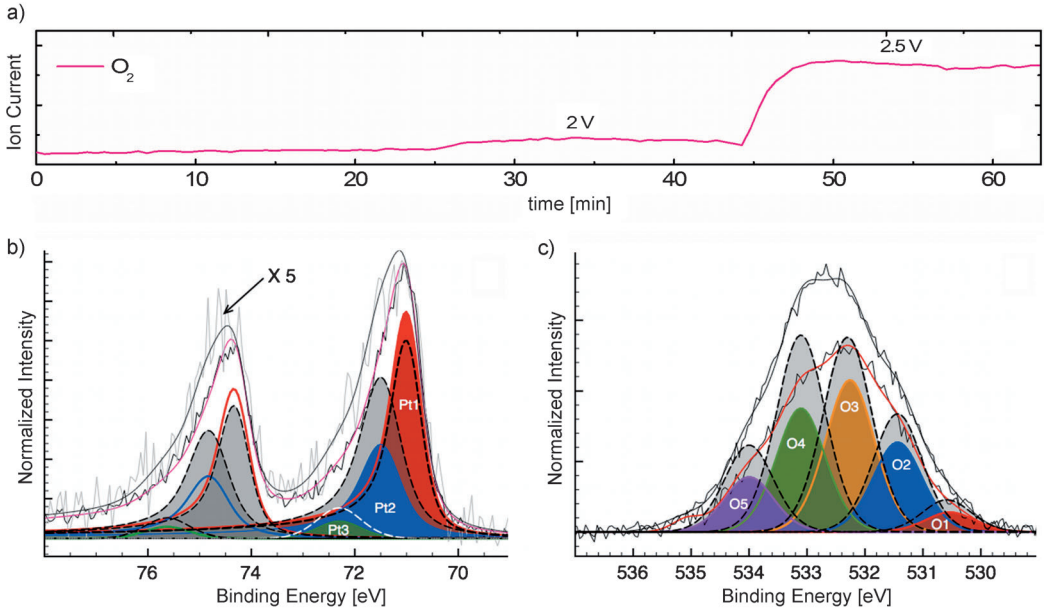

Figure 3. Pt/Nafion/Pt system: a) MS O_2 traces during the anodic polarization of the WE; XPS spectra (KE = 150 eV) corresponding to an information depth of approximately 0.5 nm. b) Deconvolved Pt4f XP spectra: red (Pt1), blue (Pt2), and green (Pt3) components for the spectrum during OER at 2 V and corresponding components at 2.5 V (dashed lines and gray shading). c) Deconvolved O1s XP spectra: components at 2 V (color code as in (b)) and components at 2.5 V (dashed lines and gray shading).

The Pt2 and Pt3 components increase in response to the increased potential (Figure 3b). The abundance of Pt2 and Pt3 is higher in the most surface-sensitive XPS measurements and decreases towards the bulk (Figure S4), establishing the interfacial character of these species. The intensity of Pt2 increases with higher OER activity, suggesting that it is related to the function of the electrode either as an active site or as an immediate reaction product. The increase of the O population leads to the evolution of the Pt3 species, which represents a divalent state of a hydrated Pt^{2+} oxide as evidenced below.

To better evaluate the involvement of the Pt^{2+} species in the OER, the WE was treated with O_3 in order to increase its oxidation state. The measured current upon anodic polarization and the corresponding Pt4f spectrum are reported in Figure 4a. The higher abundance of Pt3 and the additional components at higher BE (pale blue peak at 73.7 eV) in the Pt4f spectrum of the O_3-treated Pt film correspond to a reduction of the current at 2 V with respect to the case of the Pt film before O_3 treatment. Interestingly, increasing the potential to 4 V favors Pt reduction and correspondingly the current is significantly increased.

The current represents the OER rate: note that the Pt1/Pt2 components are lower when the OER rate is higher. These results rule out any positive effect on the presence of the Pt3 species.

Concerning the O1s spectrum, the BE chemical shift of the oxygen component of Figure 3c can be correlated to the degree of surface hydration: a shift to higher BE indicates oxygen bound to an increasing number of hydrogen atoms.

In agreement with the literature[8,15,19] the components are assigned to Pt-O (O1 at 530.4 eV), strongly bound hydroxyl groups (O2 at 531.4 eV), hydrated O:H_2O complexes (O3 at 532.2 eV), and chemisorbed H_2O (O4 at 533 eV). An additional component (O5 at 534 eV) is attributed to a multilayer film of water.[19,20] As the Pt film contains C impurities, C-O species may contribute to the components O2 and O3.[21]

With increasing the anodic potential from 2 V to 2.5 V, each O component increases (Figure 3c) but the relative abundance of the O components is differently affected by the potential as shown in (Table S1). The O4 and O5 components for molecular water increases most, while the component for the Pt-O surface (O1) increases least. Although the exact comparison for the surface O:H_2O (O3) and OH (O2) species is hampered by possible carbon impurities (Figure S6), it can be seen that their relative abundance indeed decrease as the OER is boosted. (In contrast, the absolute abundance of the C-O species increases with increasing potential in Figure S6). One can assume that their surface population is lowered due to the higher positive potential, which lowers the binding energy and favors the OER.

The relative abundance of oxygen species versus current upon potentiostatic anodic polarization for the Pt film before and after O_3 pretreatment are reported in Figure 4b. Note that the data are reported in order of increasing current but do not represent the real order of the experiments, which is reported in Figure 4a. The O_3-treated Pt film is characterized mainly by Pt-O species at 529.6 eV (O0) and at 530.4 eV (O1) and Pt-OH species at 531.4 eV (O2), while H_2O:O complexes at 532.2 eV (O3) on Pt and the molecularly chemisorbed water (O4 at 533 eV and O5 at 534 eV) are less abundant. The increase of the OER upon anodic polarization is accompanied by a decrease of the Pt-O components (O0, O1, and O2) while the abundance of O species involved in H-bonding, O3 (O:H_2O), and molecularly chemisorbed O4 and O5 species increases. A higher potential is required on oxidized Pt^{2+} in

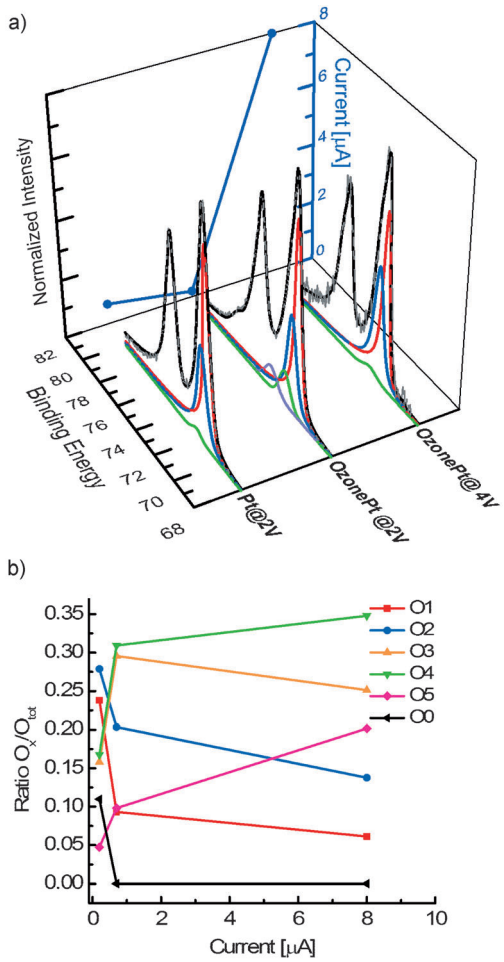

Figure 4. Pt/Nafion/Pt versus Ag wire reference electrode: A) Pt4f spectra (KE = 150 eV) during constant anodic polarization and the corresponding measured current for the sputtered Pt film WE at 2 V, and at 2 V and 4 V after pretreatment in 1 bar O_3; the order indicates chronological sequence of the experiments. b) Relative abundance of oxygen species versus current relative to the experiments in (a).

order to decrease the binding energy of the oxygen species on Pt (O0, O1 and O2) and to induce Pt reduction: on such a surface the OER is favored. The extended and stable chemisorbed O layer may prevent the chemisorption of molecular H_2O on metallic Pt and hinders the formation of Pt-O:H_2O-Pt complexes (O3) as intermediates for OER.

The results presented here give a consistent picture of the chemical dynamics of Pt in the OER reaction that brings together fragmented literature findings. The key result in the present study is the dual structure of the Pt overlayer during OER. A metallic state with oxygen often termed "surface oxide" adsorbs and dissociates water. Oxygen modification of clean Pt is a prerequisite for the dissociative adsorption of water.[23] Together with this state, a divalent hydrated Pt species also occurs with the OER activity. Tetravalent or higher oxidized species are not necessary for OER. Tetravalent hydrated Pt oxide is formed, however, as a secondary product upon extensive OER activity in an acidic electrolyte (Figure S5).

The double-layer structure of the Pt oxide formed in OER was clearly identified from electrochemical data.[24,25] It was noted that a thin highly active layer is covered by a thicker gel-like structure. It was speculated that the highly active layer should be composed of high-valent Pt oxides. This is inconsistent with the present spectroscopic data of an unprecedented surface sensitivity at high resolution of chemical states. The fact that the reacting surface is still metallic may well account for the effective discharge of the dissociated oxygen species in accordance with the electrokinetic findings. The metallic nature of highly active Pt was also recently speculated to occur in manganese oxide modified Pt systems.[26] The finding that the active layer of OER is metallic rather than oxidic has implications for the theoretical analysis of resistances.[30] It is not necessary to assume nonconventional electron transport through an oxide interface as a characteristic feature of OER. The resistivity may well arise from transport processes associated with the formation of the thick oxide layer. This is of relevance because modifications of the Pt surface could be possible that kinetically inhibit the formation of a thick layer of oxide without interfering with the function of an OER electrode. Kinetic control of the oxide stripping process[31] has indeed been observed.

The present work explains the enigmatic[24,27,30,32,33] initial reaction of Pt oxidation at ambient temperature under electrochemical control. The formation of a surface oxide electronically partly decouples the surface of the Pt metal from the electronic structure of the bulk, leading to a reduction in the density of states in the valence band as seen in the shift of the Pt4f spectrum by 0.6 eV (Figure 3b). This is prerequisite for the dissociative adsorption of water (see O1s spectra in Figure 3c and reference experiments on Pt foil in Figure S3) as well as for the mobilization of Pt.

$$Pt^{\delta} + 4\,H_2O + n\,H_2O \rightarrow [Pt(H_2O)_4]^{2+} + n\,H_2O + 2\,e^- \quad (1)$$

Reaction (1) becomes energetically feasible through the energy gain by solvation. If this is reduced by working at low pressure or in the gas phase, it can be expected that the near-surface oxide stays more stable and disintegration is reduced.

In the presence of the electrolyte the Pt aquo complex undergoes condensation according to

$$2\,[Pt(H_2O)_4]^{2+} \rightarrow [Pt_2(O)(H_2O)_6]^{2+} + 2\,H^+ + H_2O \quad (2)$$

The dimer can either continue to condense to form hydrous PtO or oxidize further to give $[Pt_2(O)_2(H_2O)_4]^{4+}$, from which hydrous PtO_2[24] and mixed-valent oxides are formed by continuing condensation. These reactions give rise to the chemically inequivalent OH and H_2O species detected in the O1s spectra of OER electrodes[34] (see Figure 3c) creating the gel structure[25,27] seen in Figure S5. Adjusting the pH of the electrolyte and kinetically disturbing the precipitation of the hydrous oxides may extend the integrity of working electrodes.

In conclusion, in this work we used in situ spectroscopy to observe the reacting interface during gas-phase water elec-

trolysis and verify its electrocatalytic function by online product analysis. It was possible to separate the transient active state of the electrode from a more stable, oxidic state that represents a deactivated state. The impact of the voltage on the OER indicates that the reaction kinetics are enhanced by the manipulation of the electrode Fermi level: stronger Pt–O bonds in stable oxidic phase induce overpotential. The present results offer the possibility that structural modifications on bare Pt may be possible that prolong the integrity of the dynamic working surface by preventing the formation of unnecessary oxide overlayers during OER.

Received: June 3, 2013
Published online: September 17, 2013

Keywords: Nafion · platinum · water electrolysis · X-ray photoelectron spectroscopy

[1] S. Trasatti, *Electrochim. Acta* **1984**, *29*, 1503 – 1512.
[2] A. Vojvodic, J. K. Norskov, *Science* **2011**, *334*, 1355 – 1356.
[3] J. Suntivich, K. J. May, H. A. Gasteiger, J. B. Goodenough, Y. Shao-Horn, *Science* **2011**, *334*, 1383 – 1385.
[4] A. J. Appleby, *Catal. Rev.* **1970**, *4*, 221 – 244.
[5] G. Centi, M. Gangeri, M. Fiorello, S. Perathoner, J. Amadou, D. Bégin, M. J. Ledoux, C. Pham-Huu, M. E. Schuster, D. S. Su, J.-P. Tessonnier, R. Schlögl, *Catal. Today* **2009**, *147*, 287 – 299.
[6] A. K. N. Reddy, M. A. Genshaw, J. O'M. Bockris, *J. Chem. Phys.* **1968**, *48*, 671.
[7] M. Peuckert, H. P. Bonzel, *Surf. Sci.* **1984**, *145*, 239 – 259.
[8] C. Ranjan et al., unpublished.
[9] Z. Zhu, F. Tao, F. Zheng, R. Chang, Y. Li, L. Heinke, Z. Liu, M. Salmeron, G. A. Somorjai, *Nano Lett.* **2012**, *12*, 1491 – 1497.
[10] J. Willsau, O. Wolter, J. Heitbaum, *J. Electroanal. Chem.* **1985**, *195*, 299 – 306.
[11] C. R. Churchill, D. B. Hibbert, *J. Chem. Soc. Faraday Trans. 1* **1982**, *78*, 2937 – 2945.
[12] M. Peuckert, *Electrochim. Acta* **1984**, *29*, 1315 – 1320.
[13] E. Rach, J. Heitbaum, *Electrochim. Acta* **1986**, *31*, 477 – 479.
[14] D. S. Austin, D. C. Johnson, T. G. Hines, E. T. Berti, *Anal. Chem.* **1983**, 55, 2222 – 2226.
[15] D. J. Miller, H. Öberg, S. Kaya, H. Sanchez Casalongue, D. Friebel, T. Anniyev, H. Ogasawara, H. Bluhm, L. G. M. Pettersson, A. Nilsson, *Phys. Rev. Lett.* **2011**, *107*, 1955021 – 1955025.
[16] L. R. Merte L. R. Merte, F. Behafarid, D. J. Miller, D. Friebel, S. Cho, F. Mbuga, D. Sokaras, R. Alonso-Mori, T.-C. Weng, D. Nordlund, A. Nilsson, B. R. Cuenya, *ACS Catal.* **2012**, *2*, 2371 – 2375.
[17] A. Knop-Gericke, E. Kleimenov, M. Hävecker, R. Blume, D. Teschner, S. Zafeiratos, R. Schlögl, V. I. Bukhtiyarov, V. V. Kaichev, I. P. Prosvirin, A. I. Nizovskii, H. Bluhm, A. Barinov, P. Dudin, M. Kiskinova, *Adv. Catal.* **2009**, *52*, 213 – 272.
[18] F. Tao, M. Salmeron, *Science* **2011**, *331*, 171 – 174.
[19] S. Yamamoto, H. Bluhm, K. Andersson, G. Ketteler, H. Ogasawara, M. Salmeron, A. Nilsson, *J. Phys.: Condens. Matter* **2008**, *20*, 184025 – 184039.
[20] T. Schiros, K. J. Andersson, L. G. M. Pettersson, A. Nilsson, H. Ogasawara, *J. Electr. Spectros. Rel. Phen.* **2010**, *177*, 85 – 98.
[21] R. Arrigo, M. Hävecker, S. Wrabetz, R. Blume, M. Lerch, J. McGregor, E. P. J. Parrott, J. A. Zeitler, L. F. Gladden, A. Knop-Gericke, R. Schlögl, D. S. Su, *J. Am. Chem. Soc.* **2010**, *132*, 9616 – 9630.
[22] Emil project: http://www.helmholtzberlin.de/pubbin/news_seite?nid=13384&sprache=en.
[23] G. B. Fisher, J. L. Gland, *Surf. Sci.* **1980**, *94*, 446 – 455.
[24] A. E. Bolzán, A. J. Arvia, *J. Electroanal. Chem.* **1992**, *341*, 93 – 109.
[25] A. E. Bolzan, A. J. Arvia, *J. Electroanal. Chem.* **1994**, *375*, 157 – 162.
[26] M. S. El-Deab, M. I. Awad, A. M. Mohammad, T. Ohsaka, *Electr. Commun.* **2007**, *9*, 2082 – 2087.
[27] M. Peuckert, H. Ibach, *Surf. Sci.* **1984**, *136*, 319 – 326.
[28] D. L. Bashlakov, L. B. F. Juurlink, M. T. M. Koper, A. I. Yanson, *Catal. Lett.* **2012**, *142*, 1 – 6.
[29] B. C. Batista, E. Sitta, M. Eiswirth, H. Varela, *Phys. Chem. Chem. Phys.* **2008**, *10*, 6686 – 6692.
[30] A. Damjanovic, V. I. Birss, D. S. Boudreaux, *J. Electrochem. Soc.* **1991**, *138*, 2549 – 2555.
[31] T. Reier, M. Oezaslan, P. Strasser, *ACS Catal.* **2012**, *2*, 1765 – 1772.
[32] J. O. Bockris, A. Huq, *Proc. R. Soc. London Ser. A* **1956**, *237*, 277 – 296.
[33] M. I. Rojas, M. J. Esplandiu, L. B. Avalle, E. P. M. Leiva, V. A. Macagno, *Electrochim. Acta* **1998**, *43*, 1785 – 1794.
[34] M. Wakisaka, Y. Udagawa, H. Suzuki, H. Uchida, M. Watanabe, *Energy Environ. Sci.* **2011**, *4*, 1662 – 1666.

